



OPEN ACCESS

EDITED BY

Chengyuan Xu,
Southwest Petroleum University, China

REVIEWED BY

Qigui Tan,
Changzhou University, China
Zhu Baiyu,
Yangtze University, China

*CORRESPONDENCE

Min Guo,
✉ guomin10@cdut.cn
Meiyan Fu,
✉ fumeiyan08@cdut.cn

SPECIALTY SECTION

This article was submitted to Advanced Clean Fuel Technologies, a section of the journal Frontiers in Energy Research

RECEIVED 04 November 2022

ACCEPTED 12 December 2022

PUBLISHED 06 January 2023

CITATION

Lan H, Guo M, Fu M, Deng H, Gluyas J, Xu W, Tang M, Wu D, Li Y and Guo H (2023), The effect of meteoric water on the very fine crystalline dolomite reservoir in the shallow burial zone: A case study of the Ma5₅ submember of Majiagou Formation in Ordos Basin. *Front. Energy Res.* 10:1089171. doi: 10.3389/fenrg.2022.1089171

COPYRIGHT

© 2023 Lan, Guo, Fu, Deng, Gluyas, Xu, Tang, Wu, Li and Guo. This is an open-access article distributed under the terms of the [Creative Commons Attribution License \(CC BY\)](https://creativecommons.org/licenses/by/4.0/). The use, distribution or reproduction in other forums is permitted, provided the original author(s) and the copyright owner(s) are credited and that the original publication in this journal is cited, in accordance with accepted academic practice. No use, distribution or reproduction is permitted which does not comply with these terms.

The effect of meteoric water on the very fine crystalline dolomite reservoir in the shallow burial zone: A case study of the Ma5₅ submember of Majiagou Formation in Ordos Basin

Haoxiang Lan¹, Min Guo^{1,2*}, Meiyan Fu^{1,2*}, Hucheng Deng^{1,2}, Jon Gluyas³, Wang Xu^{1,2}, Mingyuan Tang⁴, Dong Wu^{1,2}, Yilin Li¹ and Hengwei Guo¹

¹College of Energy, Chengdu University of Technology, Chengdu, China, ²State Key Laboratory of Oil and Gas Reservoir Geology and Exploitation, Chengdu University of Technology, Chengdu, China, ³Department of Earth Science, Durham University, Durham, United Kingdom, ⁴Exploration and Development Research Institute of North China Oil and Gas Company, Zhengzhou, China

The meteoric water has obviously changed the physical properties of dolostone reservoirs in the vertical vadose zone and the horizontal phreatic zone, but its influence on the dolostone reservoirs in the shallow burial zone beneath the phreatic surface is still unclear. This study aims to reveal the effect of meteoric water on the dolostone reservoirs in the shallow burial zone through X-ray diffraction, cathodoluminescence, C, O, and Sr isotope using the sample from Majiagou Formation in the Daniudi gas field, Ordos Basin. The diagenesis and paragenesis of the Ma 55 submember were identified and interpreted through petrological study, combined with data from electron probe, X-ray diffraction analysis, and geochemical parameters of diagenetic minerals. The color of the very fine crystalline dolomite under the cathodoluminescence is dark red and red. The order degree of dolomite ranges from 0.54 to 0.91, showing the origin of early seepage-reflux dolomitization. There are a large number of different calcite cements as fills within the pores and fractures. The color of the calcite cement under the cathodoluminescence is orange-yellow, with a zonal structure. Hydrothermal fluid during late diagenesis could be identified by the authigenic fluorite filling in the fractures. According to the assembly of diagenetic minerals, the very fine crystalline dolostones have experienced the seepage-reflux dolomitization, meteoric water dissolution, shallow burial cementation and late cementation. The void spaces of the very fine crystalline dolostones are intercrystalline pores and microfractures. Although a large number of dissolved pores and caves developed in the period of meteoric water dissolution, these caves and dissolved pores has been mostly filled by multi-stages of cementation. Therefore, the effect of meteoric water on dolostone reservoirs in the shallow burial zone beneath the phreatic surface is not obvious. The main controlling factor for the quality of dolostone reservoir was dolomitization. This study provides a new

understanding of the influence of meteoric water on reservoir quality in the shallow burial zone during the paleokarst period.

KEYWORDS

Majiagou Formation, Ordos Basin, karstification, shallow burial zone, dolomitization

1 Introduction

The Ordovician Majiagou Formation in Ordos Basin is the main target of natural gas exploration in northern China (Yang et al., 2011; Fu et al., 2017; Wei et al., 2017). Due to the influence of Caledonian and Hercynian tectonic movement, the Majiagou Formation has suffered a long-term exposure and subaerial dissolution, and displayed strong karstification (Wang et al., 2005; Li et al., 2008; Li et al., 2017; Fu et al., 2019; Xie K. et al., 2020). Karstification refers to the subaerial dissolution of carbonate by meteoric water during the period of the sediment's consolidation or the exposure of buried carbonate rocks. The contribution of the karstification to the oil and gas reservoir quality is widely discussed, based on the research of paleogeomorphologic features, unconformities and fault development (Wennberg et al., 2016; Zhang et al., 2016; Wei et al., 2018; Xiao et al., 2019; Ding et al., 2020; Jiu et al., 2021; Liu et al., 2021; Retana et al., 2021; Yang M. Y. et al., 2021). The vertical section of karstification can be divided into surface karst zone, vertical vadose zone and horizontal phreatic zone (Jiang and Jin, 2009; Qu et al., 2015; Zhu et al., 2018; Zhao et al., 2019). The vadose and phreatic zones occurred in karstification sections result from the meteoric water flowed under the influence of gravity. According to the differences of paleogeomorphology, karstification can be divided into several types of karst units (Esteban and Feng, 1991). It is generally believed that the degree of karstification of karst highlands and karst slopes is stronger than other karst units and the carbonate rocks in above two units are prone to form reservoirs with high quality (Chen et al., 2007; Zhang et al., 2021; Zhu et al., 2021).

At present, the natural gas exploitation of the Ma5 member of the Majiagou Formation located in the karst highlands and karst slopes in the Daniudi area of Ordos Basin is significant, with the average yield of $2.4 \times 10^4 \text{ m}^3/\text{d}$. The Ma5 member has been divided into 10 submembers. Among the 10 submembers, the Ma5₁ to Ma5₄ submembers are located in the vadose zone and horizontal phreatic zone (He et al., 2013; Sun, 2020; Xie R. C. et al., 2020; Yu et al., 2020; Xu et al., 2021), while the Ma5₅ submember is distributed in the shallow burial zone. The Ma5₅ submember is composed of dolostone and limestone. The mechanism of microbial dolomitization in the middle and lower of the Ma5 member is reported in the central and eastern Ordos Basin (Liu et al., 2017; Yang W. et al., 2021; Luo et al., 2022). The dolostones in the Daniudi area are distributed in the shallow burial zone beneath the phreatic surface, where may be influenced by meteoric water. Study on the genesis of dolostone in the shallow burial zone beneath the phreatic

surface during the paleokarst period will improve to understand the development of high-quality dolomite reservoir in this area. In this study, taking dolostones in the Ma5₅ submember as an example, based on the lithofacies observation, X-ray diffraction analysis, the measurement of carbon, oxygen and strontium isotope, the influence of meteoric water on the dolostone reservoir of the Ma5₅ submember in the shallow burial zone beneath the phreatic surface was discussed.

Study on the genesis of dolostone in the shallow burial zone beneath the phreatic surface enables us to better understand how to identify the distribution of high-quality dolostone reservoir in the deep layers. This study will help to further enhance the exploration of deep natural gas favorable areas.

2 Geological setting

The main structural units of the Ordos Basin include Yimeng uplift, Jinxi fold, northern Shaanxi sag, Yishan slope, central paleo-uplift, Tianhuan sag, western margin thrust belt and Weibei uplift (Hou et al., 2003; He et al., 2013). The basin was composed of Caledonian foreland basin and Helan rift at the same time in early Paleozoic. During the sedimentary period of the Majiagou Formation, Helan rift warped in the western margin of the basin, forming a central paleo-uplift, and the Northern Shaanxi sag formed in the east of the basin (Figure 1). These two tectonic units control the Ordovician palaeogeomorphological configuration (He et al., 2013). Under the influence of the Caledonian Orogeny, the North China platform uplifted at the end of the Middle Ordovician, resulting in a sedimentary interruption of about 130 Ma. In the late Ordovician-early Carboniferous, the sea level declined, and the large-scale regression led to the long-term exposure and denudation of the Ordovician carbonate strata. The sedimentary strata of the basin were also absent during this period, and the weathering crust developed widely under the strong karstification. So far, the weathering crust of Ordovician carbonate strata has been basically formed, which facilitates the development of karst reservoirs in the Majiagou Formation.

Daniudi gas field is located in the northeastern Yishan slope (Figure 1). The Majiagou Formation in the study area can be divided into five members from bottom to top, namely Ma1-Ma5 members. There was many times of transgressions and regressions, while retrogression occurred in the depositional period of Ma1, Ma3 and Ma5 members, and transgression occurred in the depositional period of Ma2 and

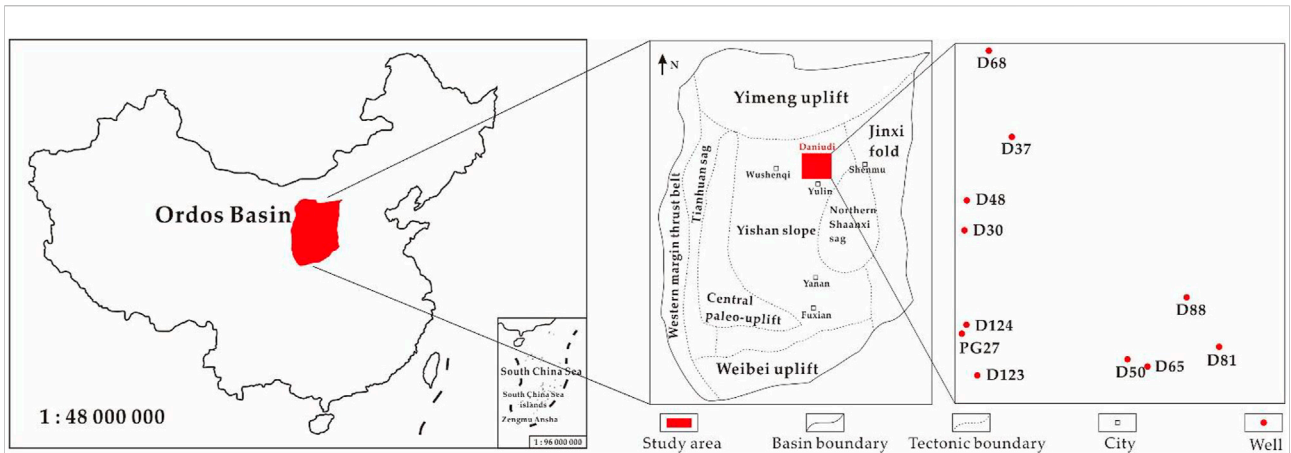


FIGURE 1 Location of the study area (Adopted from Hou, et al., 2003).

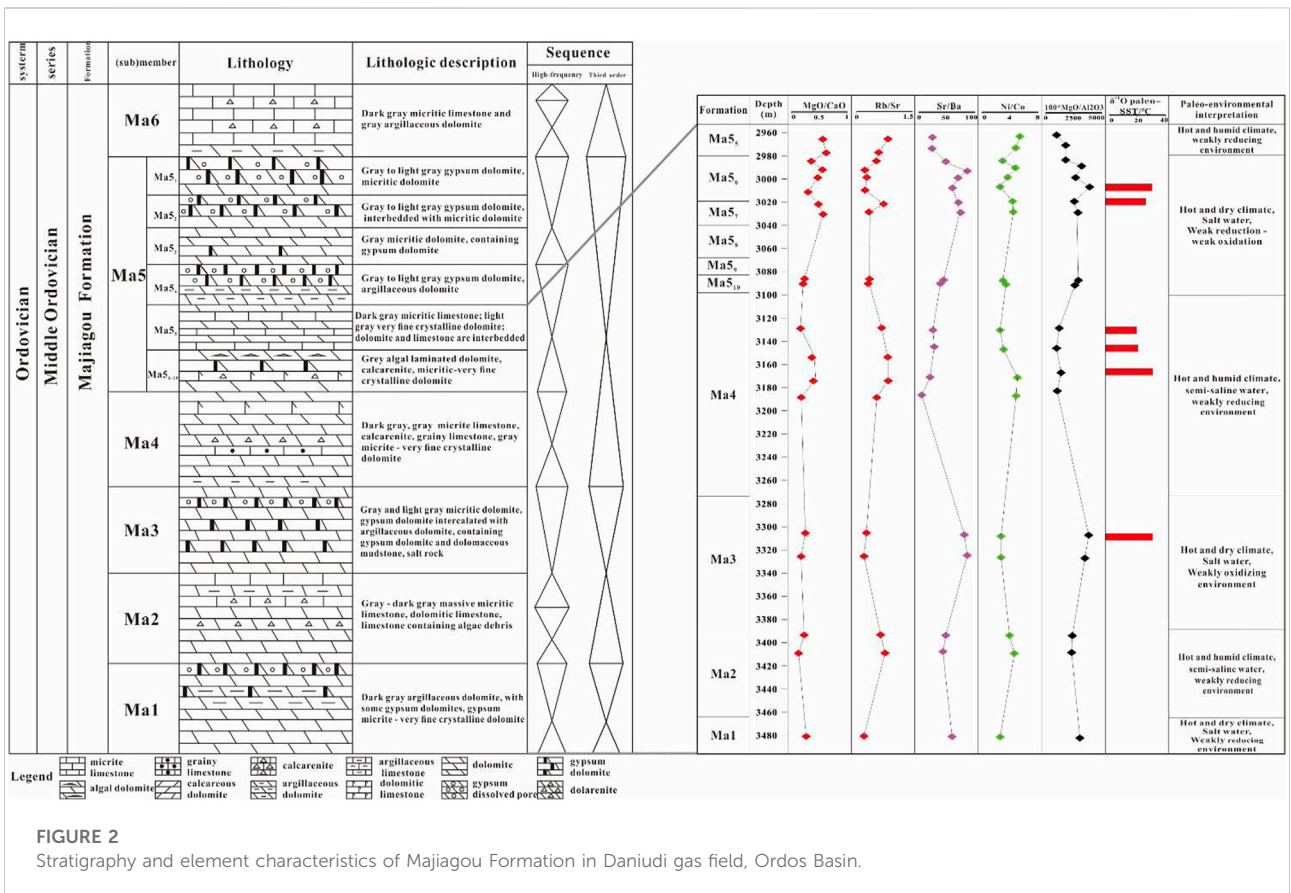


FIGURE 2 Stratigraphy and element characteristics of Majiagou Formation in Daniudi gas field, Ordos Basin.

Ma4 members. The transgression during the depositional period of Ma4 member reached the maximum (Feng et al., 2004). Controlled by the change of sea level, the sedimentary facies of the Majiagou Formation evolved from restricted platform to evaporative platform, and there were several sets of gypsum rock

and salt rock interbedded with dolostones (Figure 2). The Ma5 member can be divided into 10 submembers. Ma5₇₋₁₀ submembers deposited on the dolomitic tidal flat, containing very fine crystalline dolomites. During the depositional period of the Ma5₆ submember, the content of terrigenous mud increased

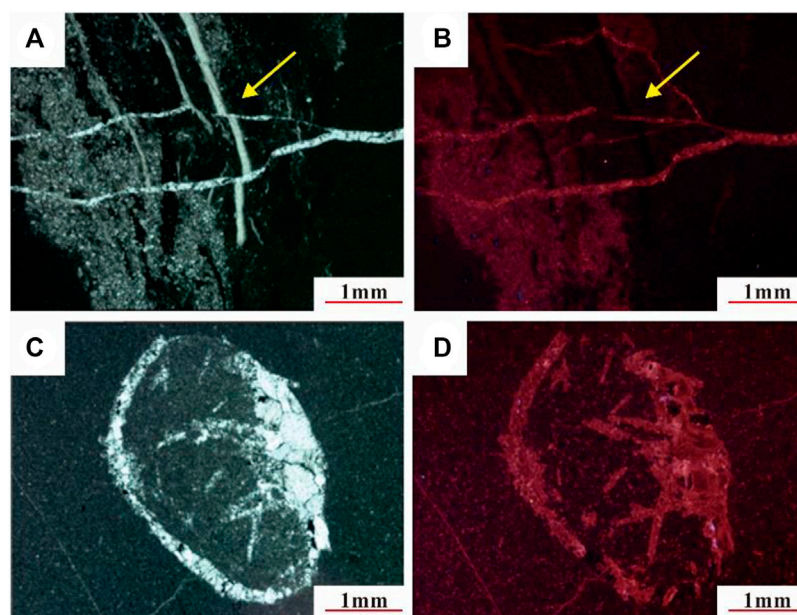


FIGURE 3

Microscopic and cathodoluminescence characteristics of limestone. (A) Well D1-530, 3105.53 m, tectonic fractures cut the bioclast (yellow arrow); (B) Cathodoluminescence photos of figure a, the luminescence color of calcite filled in fractures is bright orange; (C) Well D88, 2816.62 m, the mold pore is filled with tabular gypsum, replaced by calcite; (D) Cathodoluminescence photos of figure c, the luminescence of calcite is bright orange.

in the sediments. However, the crystalline dolomites are still the main minerals in the Ma₅ submember. The weathering crust mainly refers to Ma₅₁₋₄ submembers in the whole Ordos Basin. Particularly, the karst breccias could be observed in the Ma₅₁₋₅ submembers.

3 Sampling and testing methods

Sample source: In this study, the rock samples of the Ma₅ submember of the Majiagou Formation in the Daniudi gas field were collected from 13 wells. The location of the sampling wells is shown in Figure 1. A total of 104 samples are analyzed, including 24 plunger cores and 80 broken samples. The whole rock X-ray diffraction detection, major and trace elements measurement, C, O, Sr isotopes and rare earth elements analysis were performed in the State Key Laboratory of Oil and Gas Reservoir Geology and Exploitation in China. 27 thin sections were observed by cathodoluminescence microscope.

Testing method: XRD analysis was performed according to the SY/T 5163–2010 standard (China): the samples were cleaned until the fluorescence level is below Grade IV, and dried in a drying oven at 60°C. After drying, break the samples into 1 mm, and then grind them to 40 μm. The instrument of XRD analysis is Rigaku XRD/Rigaku Ultima IV instrument of Japanese physics, with operating voltage of 30 kV, current of 20 mA and scanning

speed of 2°/min. Major, trace and rare earth elements were determined by PE 5300 V inductively coupled plasma atomic emission spectrometer (ICP-OES) and Agilent Technologies 7700 Series ICP-MS. Rare earth elements were standardized using North American shale (Gromet et al., 1984). Major elements were determined by GB/T 14506-2010 industry standard part 28 in China, trace and rare earth elements were determined by GB/T 14506-2010 industry standard part 29 in China. The C and O isotopes were determined by the MAT253 stable isotope ratio mass spectrometer of Thermo Science, United States. Isotope determination was performed according to SY/T 5238-2008 industry standard (China). The measurement accuracy of ¹³C was 0.0037‰, and that of ¹⁸O was 0.013‰. Cathodoluminescence analysis was performed on British CITL MK2-5, with the polarizing microscope produced by Germany Leica DM4500, with the voltage of 14 kV, the current of 380 μA, and exposure time of 12 s.

4 Results

4.1 Lithology

4.1.1 Limestone

The color of the limestone is light gray to gray. Lithologically, the limestone in the study area is micritic limestone. There are

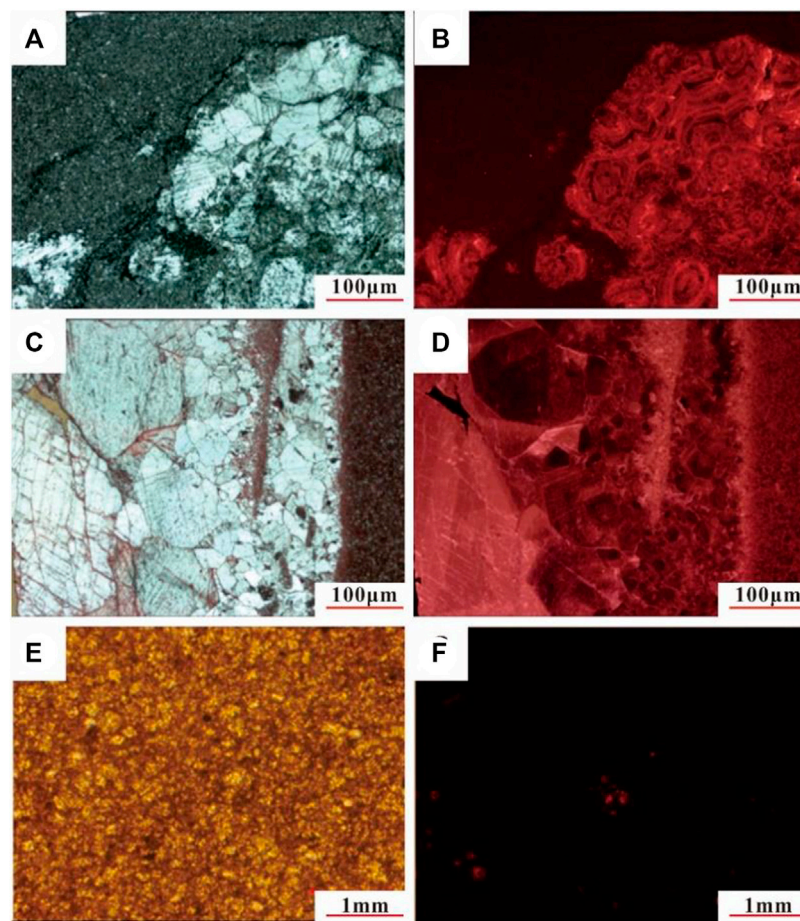


FIGURE 4

Microscopic and cathodoluminescence characteristics of dolomite. (A) Well PG27, 2979.52m, calcite cementation in the vugs; (B) Cathodoluminescence photos of figure a, calcite with zonal luminescence characteristic; (C) Well D48, 3022.17 m, coarse crystalline calcite filling the fracture; (D) Cathodoluminescence photos of figure c, the calcite without zonal luminescence characteristics; (E) Well D48, 3014.88 m, very fine crystalline dolomite; (F) Cathodoluminescence photos of figure e, the luminescence of dolomite is not obvious.

two types of fractures can be observed on the cores: tectonic fractures and weathering fractures. The tectonic fractures cut the fossils as seen under the microscope (Figures 3A, B), and these fractures are filled with calcite. The crystal shape of gypsum could be observed in Figure 3C, however, the gypsum was replaced by calcite according to interference colors under cross-polarized light and cathodoluminescence (Figures 3C, D).

4.1.2 Dolomite

The mineral composition detected by XRD shows that the main mineral of the dolomite samples from Ma5₃ submember is dolomite, followed by calcite, with an average content of 94.4% and 3.7%, respectively. According to the crystal size of dolomites, the dolostones can be divided into micritic dolostone and very fine crystalline dolostone. The calcareous dolostone is a transitional lithology, and its cathodoluminescence color is

non-luminescent or dark red light. The color of micritic dolostone on the hand specimen is dark gray or gray black. Weathering fractures and gypsum are visible under the microscope. The calcites filled within the pores and fractures have multiphase crystallization, identified by cathodoluminescence. The early phase was the fine crystalline calcite with zonal luminescence characteristics (Figures 4A, B) in the vugs. The late phase was calcite without zonal luminescence characteristics (Figures 4C, D). There are almost no visible pores in the micritic dolostone. The color of very fine crystalline dolostone on the hand specimen is gray, with fewer fractures compared with above two lithologies. The dolomite crystal size of the dolostone under microscope is between 50 and 100 µm. The crystal morphology of this dolostone is more regular than micritic dolostone, which is euhedral to subhedral. The cathodoluminescence color of very fine crystalline dolostone is

TABLE 1 C and O isotope of carbonate rocks from the Ma5_s submember.

Well	Sample no.	Depth(m)	Lithology	$\delta^{13}\text{C}_{\text{V-PDB}}\text{‰}$	$\delta^{18}\text{O}_{\text{V-PDB}}\text{‰}$
D1-530	9/52	3097.42	very fine crystalline dolomite	-0.13	-6.75
D1-530	36/52	3101.42	very fine crystalline dolomite	-0.16	-8.09
D1-530	41/67	3108.28	very fine crystalline dolomite	-0.28	-7.47
D1-530	5/36	3112.78	very fine crystalline dolomite	-0.30	-7.40
D1-530	25/36	3115.62	very fine crystalline dolomite	-0.11	-7.52
PG27	31/47	2987.35	very fine crystalline dolomite	-0.06	-7.27
D1-530	31/67	3106.75	Micrite dolomite	-1.48	-7.10
PG27	27/49	2978.11	Micrite dolomite	-0.46	-6.34
PG27	36/49	2979.52	Micrite dolomite	-0.53	-7.01
PG27	11/47	2983.72	Micrite dolomite	-0.76	-7.22
D48	5/99	3009.32	Calcareous dolomite	-0.38	-8.18
D48	26/99	3013	Calcareous dolomite	-1.77	-8.43
D81	30/71	2846.68	Calcareous dolomite	-0.65	-7.53
D48	5/99	3009.32	Calcite vein	-2.17	-14.01
D48	26/99	3013	Calcite vein	-3.76	-13.59
D48	56/99	3018.46	Calcite vein	-2.78	-16.01
D48	75/99	3022.05	Calcite vein	-2.54	-14.18
D88	9/83	2815.73	Calcite vein	-3.72	-14.47
D88	21/83	2817.02	Calcite vein	-4.27	-14.34

TABLE 2 Sr isotope of carbonate rocks from the Ma5_s submember.

Well	Sample no.	Depth(m)	Lithology	$^{87}\text{Sr}/^{86}\text{Sr}$
D1-530	9/52	3097.42	very fine crystalline dolomite	0.709711
D1-530	36/52	3101.42	very fine crystalline dolomite	0.709783
D1-530	41/67	3108.28	very fine crystalline dolomite	0.709579
D1-530	5/36	3112.78	very fine crystalline dolomite	0.709766
D1-530	25/36	3115.62	very fine crystalline dolomite	0.710010
PG27	31/47	2987.35	very fine crystalline dolomite	0.709358
D1-530	31/67	3106.75	Micrite dolomite	0.710430
PG27	36/49	2979.52	Micrite dolomite	0.709561
D48	5/99	3009.32	Calcareous dolomite	0.709228
D48	26/99	3013	Calcareous dolomite	0.709118
D48	99/99	3026.35	Limestone	0.709504
D67	21/48	2892.28	Limestone	0.709082

TABLE 3 The composition of elements in carbonate rocks from the Ma5₅ submember.

Well	Sample no.	Depth(m)	Lithology	CaO %	MgO %	K ₂ O %	Na ₂ O %	Al ₂ O ₃ %	TFe ₂ O ₃ %	Mn × 10 ⁻³
D1-530	9/52	3097.42	very fine crystalline dolomite	31.721	22.120	0.051	0.062	0.186	0.213	0.070
D1-530	36/52	3101.42	very fine crystalline dolomite	34.362	19.180	0.080	0.060	0.264	0.266	0.080
D1-530	41/67	3108.28	very fine crystalline dolomite	32.538	21.020	0.101	0.063	0.332	0.298	0.070
D1-530	5/36	3112.78	very fine crystalline dolomite	31.863	19.760	0.079	0.060	0.286	0.337	0.080
D1-530	25/36	3115.62	very fine crystalline dolomite	30.239	19.370	0.287	0.064	1.051	0.390	0.080
PG27	31/47	2987.35	very fine crystalline dolomite	29.726	20.330	0.056	0.054	0.221	0.260	0.080
D1-530	31/67	3106.75	Micrite dolomite	26.277	19.220	1.023	0.079	3.351	0.991	0.190
PG27	27/49	2978.11	Micrite dolomite	28.710	20.350	0.074	0.050	0.308	0.373	0.261
PG27	36/49	2979.52	Micrite dolomite	29.811	20.730	0.080	0.054	0.302	0.199	0.060
PG27	11/47	2983.72	Micrite dolomite	28.580	19.960	0.213	0.052	0.763	0.501	0.251
D48	5/99	3009.32	Calcareous dolomite	37.744	13.060	0.082	0.053	0.293	0.234	0.080
D48	26/99	3013	Calcareous dolomite	38.352	10.530	0.061	0.053	0.211	0.224	0.080
D81	30/71	2846.68	Calcareous dolomite	43.750	9.048	0.056	0.038	0.143	0.111	0.078
D48	99/99	3026.35	Limestone	49.362	1.606	0.075	0.048	0.288	0.110	0.040
D67	21/48	2892.28	Limestone	52.953	0.250	0.057	0.056	0.247	0.103	0.060

non-luminescent to dark red light (Figures 4E, F). There are a small number of intercrystalline pores and intercrystalline dissolved pores developed in the very fine crystalline dolomite.

4.2 Carbon and oxygen isotope

The compositions of C and O isotopes are shown in Table 1. The $\delta^{13}\text{C}_{\text{V-PDB}}$ values of the very fine crystalline dolomite ranged from -0.30 to -0.06‰ , with an average of -0.17‰ , and the $\delta^{18}\text{O}_{\text{V-PDB}}$ values ranged from -8.09 to -6.75‰ , with an average of -7.42‰ . The $\delta^{13}\text{C}_{\text{V-PDB}}$ values of micritic dolomites range from -1.48 to -0.46‰ , with an average of -0.81‰ ; the $\delta^{18}\text{O}_{\text{V-PDB}}$ values range from -7.22 to -6.34‰ , with an average of -6.91‰ . The $\delta^{13}\text{C}_{\text{V-PDB}}$ values of the calcareous dolomite range from -1.77 to -0.38‰ , with an average of -0.93‰ , and the $\delta^{18}\text{O}_{\text{V-PDB}}$ range from -8.43 to -7.53‰ , with an average of -8.05‰ . The $\delta^{13}\text{C}_{\text{V-PDB}}$ values of limestone ranged from -0.88 to -0.46‰ with an average of -0.67‰ , and the $\delta^{18}\text{O}_{\text{V-PDB}}$ values ranged from -9.68 to -9.57‰ with an average of -9.63‰ . The $\delta^{13}\text{C}_{\text{V-PDB}}$ value of weathering fracture filling calcite ranges from -4.27 to -2.17‰ , with an average of -3.21‰ , and the $\delta^{18}\text{O}_{\text{V-PDB}}$ value ranges

from -16.01 to -13.59‰ , with an average of -14.43‰ . The C and O isotopic values of limestone are similar with those of the Early-Middle Ordovician marine limestone (Veizer et al., 1999), and the C and O isotopic values of micritic dolomite are similar with those of the early Ordovician seawater cements ($\delta^{13}\text{C}_{\text{V-PDB}} -1.5 \sim -0.5\text{‰}$, $\delta^{18}\text{O}_{\text{V-PDB}} -6.5 \sim -5.5\text{‰}$ (Popp et al., 1986)), and the $\delta^{13}\text{C}$ value of very fine crystalline dolomite is not very negative. With the increase of the calcite percentage in whole rock, the $\delta^{18}\text{O}$ value decreases, and the calcite vein has the lightest C and O isotope value.

4.3 Sr isotope

The Sr isotope of 12 samples from 4 wells are shown in Table 2. The $^{87}\text{Sr}/^{86}\text{Sr}$ ratio of limestone ranges from 0.7091 to 0.7095, with an average of 0.7093. The distribution range of calcareous dolomite is 0.7091–0.7092, with an average of 0.7092. Micritic dolomite ranges from 0.7096–0.7104, with an average of 0.7100; Very fine crystalline dolomite ranges from 0.7094–0.7100 with an average of 0.7097. The range of 0.7086–0.7096 is taken as the standard reference range for the $^{87}\text{Sr}/^{86}\text{Sr}$ ratio of the Middle and Lower Ordovician (Veizer et al.,

TABLE 4 Rare earth element in carbonate rocks from the Ma5₃ submember.

Well	Depth (m)	Lithology	La	Ce	Pr	Nd	Sm	Eu	Gd	Tb	Dy	Ho	Er	Tm	Yb	Lu
			(×10 ⁻⁶)													
D1-530	30970.42	very fine crystalline dolomite	1.007	1.904	0.237	0.831	0.177	0.027	0.141	0.021	0.140	0.021	0.068	0.009	0.069	0.007
D1-530	31010.42	very fine crystalline dolomite	1.889	3.864	0.471	1.734	0.284	0.059	0.257	0.038	0.196	0.035	0.104	0.010	0.100	0.011
D1-530	31080.28	very fine crystalline dolomite	0.870	1.626	0.201	0.800	0.156	0.031	0.132	0.024	0.115	0.026	0.063	0.009	0.081	0.014
D1-530	31120.78	very fine crystalline dolomite	1.398	2.638	0.319	1.187	0.214	0.05	0.175	0.030	0.175	0.031	0.081	0.013	0.097	0.014
D1-530	31150.62	very fine crystalline dolomite	1.347	2.306	0.297	1.141	0.206	0.046	0.221	0.034	0.190	0.038	0.105	0.015	0.117	0.016
PG27	29870.35	very fine crystalline dolomite	0.555	1.197	0.173	0.663	0.141	0.025	0.129	0.020	0.129	0.025	0.074	0.008	0.083	0.012
D1-530	31060.75	Micrite dolomite	13.115	29.416	3.174	12.194	2.363	0.475	2.177	0.339	1.879	0.414	1.097	0.181	1.061	0.164
PG27	29780.11	Micrite dolomite	1.001	1.771	0.209	0.905	0.233	0.035	0.196	0.031	0.202	0.040	0.12	0.02	0.305	0.022
PG27	29790.52	Micrite dolomite	0.761	1.505	0.196	0.794	0.189	0.037	0.146	0.027	0.137	0.029	0.097	0.01	0.101	0.014
PG27	29830.72	Micrite dolomite	1.729	2.352	0.256	1.018	0.201	0.039	0.194	0.030	0.196	0.040	0.127	0.021	0.300	0.029
D48	30090.32	Calcareous dolomite	1.865	4.231	0.530	2.036	0.362	0.059	0.309	0.050	0.252	0.052	0.153	0.023	0.167	0.018
D48	3013	Calcareous dolomite	1.905	3.852	0.474	1.696	0.285	0.063	0.261	0.046	0.228	0.049	0.135	0.022	0.144	0.019
D81	28460.68	Calcareous dolomite	6.340	8.152	0.793	2.722	0.364	0.056	0.048	0.309	0.213	0.039	0.091	0.015	0.254	0.012
D48	30260.35	Limestone	3.878	6.799	0.820	2.944	0.475	0.098	0.450	0.068	0.335	0.063	0.146	0.021	0.153	0.019
D67	28920.28	Limestone	1.699	3.208	0.374	1.275	0.227	0.048	0.188	0.029	0.173	0.038	0.097	0.014	0.120	0.016

TABLE 5 Mineral composition and order degree of dolomite data of carbonate rocks from the Ma5_s submember.

Well	Depth (m)	Lithology	Quartz %	Plagioclase	RockSalt %	Anhydrite %	Dolostone %	Calcite %	Pyrite %	Clay %	Order degree of dolomite
D1-530	3097.42	very fine crystalline dolomite	1.2	0	0	0	96.6	2.2	0	0	0.91
D1-530	3101.42	very fine crystalline dolomite	0.8	0	0	0	89.3	9.9	0	0	0.88
D1-530	3106.75	Micrite dolomite	4.7	0	0	0	89.2	0.3	0.6	5.2	0.63
D1-530	3108.28	very fine crystalline dolomite	0.3	0	0	0	96.1	3.5	0.1	0	0.83
D1-530	3112.78	very fine crystalline dolomite	0.6	0.4	0	0	93.9	5.2	0	0	0.74
D1-530	3115.62	very fine crystalline dolomite	0.5	0.3	0	0	94.3	4.6	0.2	0	0.79
D48	3016.05	very fine crystalline dolomite	0.9	0	—	0	92.6	6.5	0	0	0.62
PG27	2987.35	very fine crystalline dolomite	0.2	0.4	0	0	97.4	2.0	0	0	0.83
PG27	2979.52	Micrite dolomite	0.8	0.4	0	0	96.3	2.4	0	0	0.83
PG27	2983.96	Micrite dolomite	0.6	0.3	—	0	98.2	0.8	0.1	0	0.82
D48	3009.32	Calcareous dolomite	0.3	0	0	0	66.2	33.5	0	0	0.79
D48	3013	Calcareous dolomite	0.4	0	0	0	59.0	40.6	0	0	0.80
D48	3020.38	Calcareous dolomite	0.3	0	—	0	54.5	45.2	0	0	0.68
D81	2846.68	Calcareous dolomite	0.3	0.2	—	0	50.1	49.4	0	0	0.74

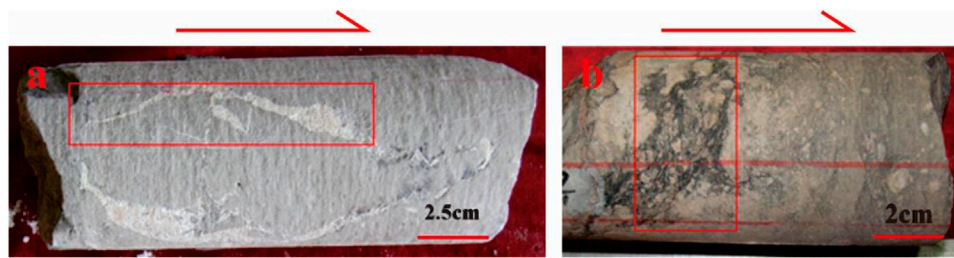


FIGURE 5

Characteristics of different karst zone on cores, the arrow indicates the vertical direction. (A) Well D87, Ma₅₂, calcite filled near vertical karst fractures, showing the characteristics of vertical vadose zone; (B) DP93H well, Ma₅₃₋₄, horizontal muddy strips containing fine breccias, indicating horizontal movement of karst water.

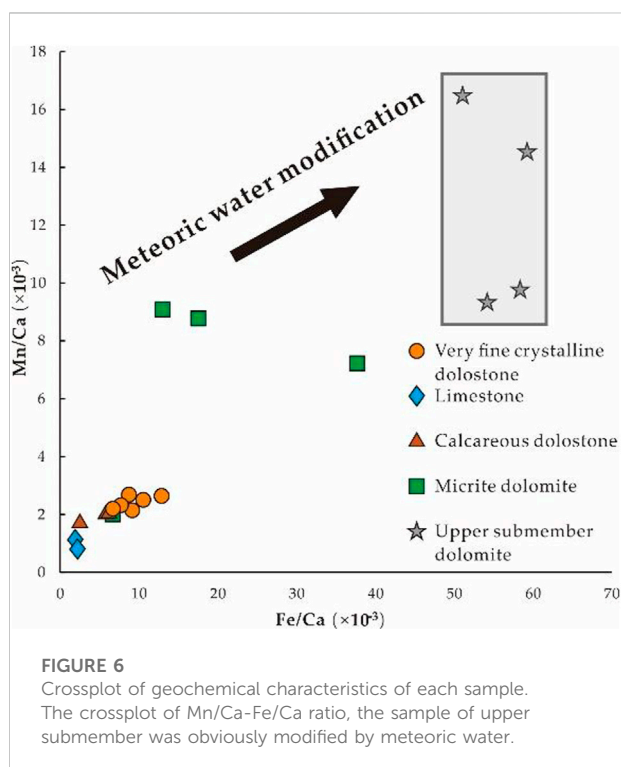


FIGURE 6

Crossplot of geochemical characteristics of each sample. The crossplot of Mn/Ca-Fe/Ca ratio, the sample of upper submember was obviously modified by meteoric water.

1999), and the $^{87}\text{Sr}/^{86}\text{Sr}$ ratio of the limestone in the study area is similar to the $^{87}\text{Sr}/^{86}\text{Sr}$ ratio of contemporary seawater. The $^{87}\text{Sr}/^{86}\text{Sr}$ ratio of most micritic dolomites and some very fine crystalline dolomites are beyond the above reference range, and the $^{87}\text{Sr}/^{86}\text{Sr}$ of micritic dolomite is the highest, followed by very fine crystalline dolomite.

4.4 Major element

The composition of major and trace elements of carbonate rocks from the Ma₅ submember are shown in Table 3. The average CaO content of very fine crystalline dolomite is

31.74%, the average MgO content is 20.30%, and that of micritic dolomite are 28.34% and 20.07%, respectively. The Ca content of very fine crystalline dolomite is higher than that of micritic dolomite, and the Mg content is slightly higher than that of micritic dolomite. The average Ca and Mg content of the calcareous dolomite were 39.95% and 10.88%, that of limestone was 51.16% and 0.93%, respectively. The Mg/Ca value of the micritic dolomite was 0.71, and that of the very fine crystalline dolomite was 0.64. The contents of Fe and Mn in the samples varied greatly. There are highest Fe and Mn contents in the micritic dolomite, with an average value of 0.52% and 125 ppm. The Fe and Mn content in the very fine crystalline dolomite is 0.29% and 77 ppm, respectively. The average values of limestone are 0.11% and 50 ppm. The Fe and Mn contents decreased with the increase of calcite percentage in whole rock. Mn/Ca values of all samples in the Ma₅ submember are closer to that of meteoric water value with 1.33 (Huang, 1990). The content of Sr in the micritic dolomite is 59.49 ppm, and that in very fine crystalline dolomite is 57.35 ppm, that in limestone is 86.20–105.91 ppm. Meanwhile, the content of Sr increases with the increase of calcite percentage in whole rock. The overall content of Na element in the sample is low. The content of K element decreases in sequence from micritic dolomite, very fine crystalline dolomite, calcite dolomite and limestone, which is consistent with the distribution characteristics of Al content. Therefore, it is inferred that the distribution of K and Al are related to the content of clay minerals.

4.5 Rare earth element

As shown in Table 4, it can be seen that the dolomite is enriched in light rare earth elements but poor in heavy rare earth elements. The composition of rare earth element fluctuates slightly. The distribution pattern of rare earth elements of dolomite is similar to micritic limestone, but the total rare earth element contents are lower than micritic limestone. The

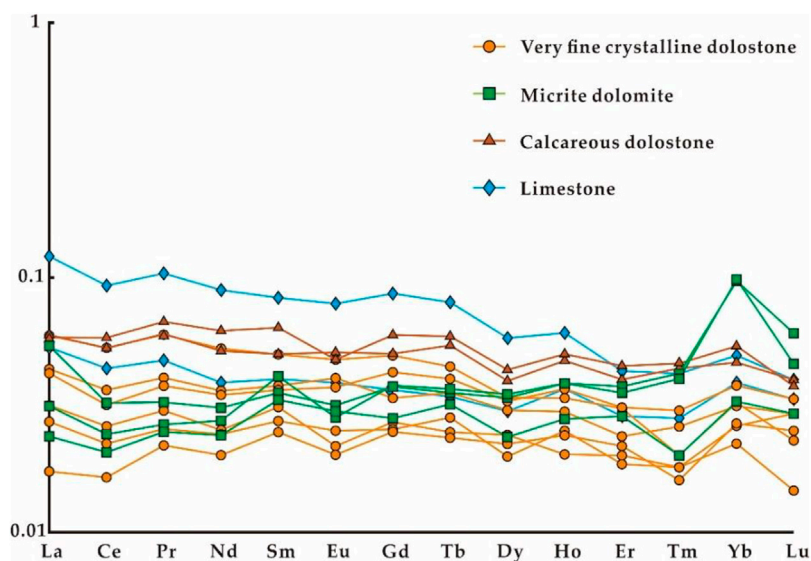


FIGURE 7
The distribution of REEs pattern of the carbonate rocks of the Ma5₅ member.

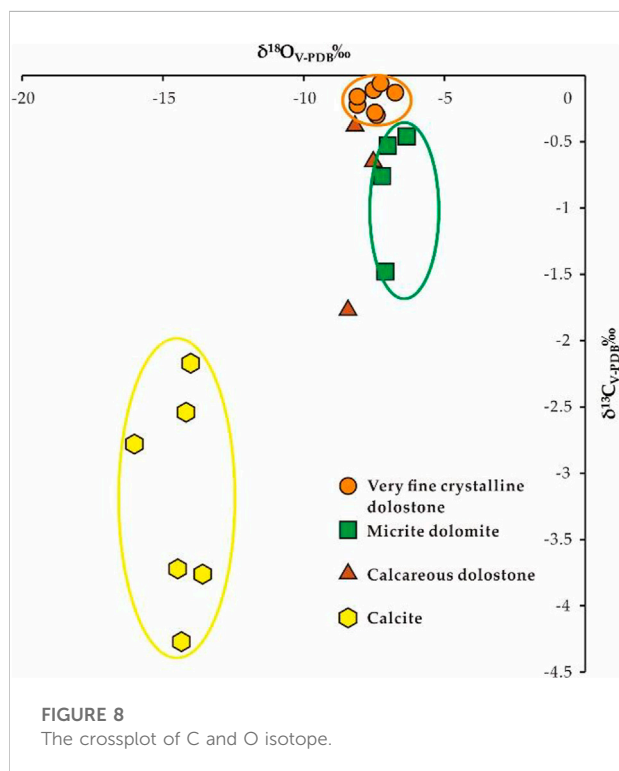


FIGURE 8
The crossplot of C and O isotope.

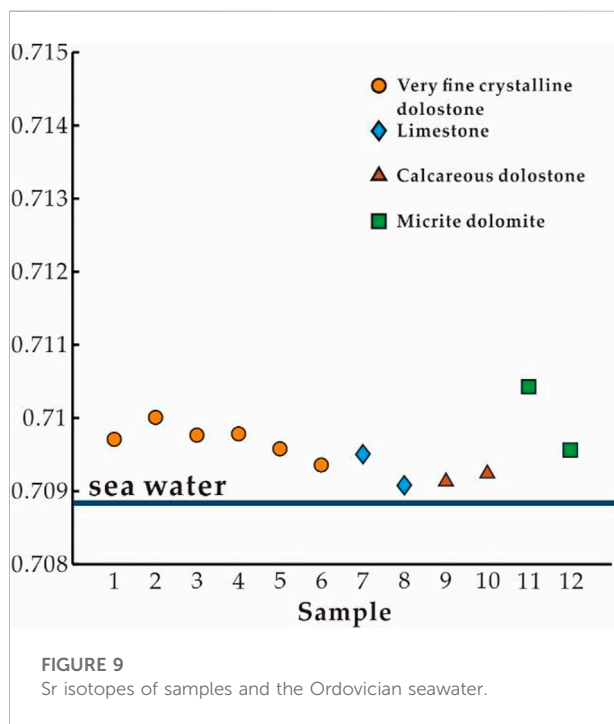
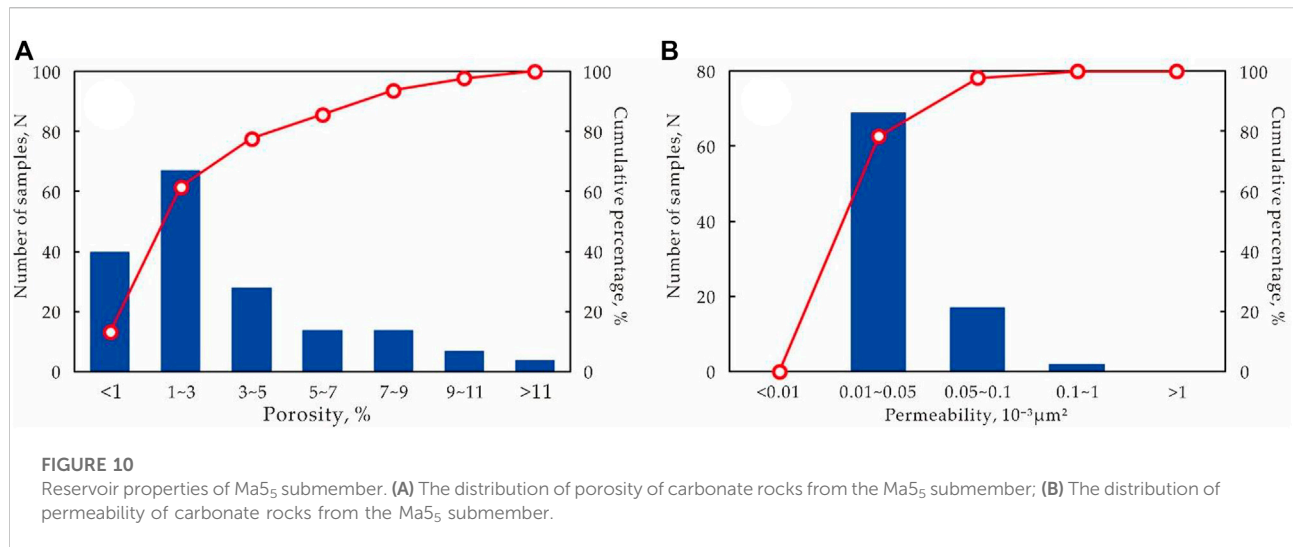


FIGURE 9
Sr isotopes of samples and the Ordovician seawater.

average δEu value of very fine crystalline dolomite is 0.21, and the average δCe value is 3.09. The average δEu value of micritic dolomite is 0.20, and the average δCe value is 3.01.

4.6 Mineral composition and order degree of dolomite

The X-ray diffraction data of the whole rock show that the content of clay minerals in the dolostone and calcareous



dolomite in the Ma₅ submember is relatively small (Table 5). There is a small amount of clay minerals in the micritic dolomite, with the content of 1.73%, which is consistent with the changes in the content of K and Al mentioned above. There are most abundant terrigenous materials in the micritic dolostones. The contents of quartz and plagioclase are 2.03% and 0.23% in the micritic dolostones, and that in the very fine crystalline dolomite is 0.64% and 0.16%, respectively. Pyrite only occurred in the micritic dolostones and very fine crystalline dolostones. The order degree of dolomite in the micritic dolostones ranges from 0.63 to 0.83, with an average of 0.76. The order degree of dolomite in the very fine crystalline dolomite ranges from 0.62 to 0.91, with an average of 0.80. The order degree of dolomite in the calcareous dolomite is similar to that of micritic dolomite with an average of 0.75.

5 Discussion

5.1 The characteristic of dolostones of the Ma₅ submember in the shallow burial zone and dolomitization

Due to different depth of stratum penetrated by meteoric water and diagenetic fluids, the intensity of karstification is different. According to the infiltration depth of meteoric water, the karstification zones are vertically divided into vadose zone and phreatic zone. Previous authors classified the Ma_{5₁₋₂} submember as a vertical vadose zone and the Ma_{5₃₋₄} submember as a horizontal phreatic zone (Lei et al., 2010; He et al., 2013). Ma_{5₁₋₂} submember in this study area mainly develop weathering fractures with high angles (Figure 5A), and nearly horizontal muddy strips containing fine breccias could be observed in the Ma_{5₃} submember (Figure 5B).

In the shallow burial zone beneath the phreatic surface, meteoric water was not easy to penetrate. Therefore, the movement of meteoric water in the shallow burial zone is very slow. In the study area, Ma₅ submember is beneath the ancient phreatic surface. Comparison with the elemental composition of dolostones from the Ma_{5₂₋₃} submembers (Figure 6), it is considered that the dolostones of the Ma₅ submember were generally consistent with the characteristics of shallow burial zone. The contents of Mg, Ca, Fe, Mn and rare earth elements in the rock are commonly used for the analysis of the intensity of karstification. Because meteoric water is rich in Fe and Mn elements (Muech and Sintubin, 1998; Henry et al., 1999), the contents of Fe and Mn elements can reflect the modification degree of meteoric water. The carbonate rocks deposited in the Ma_{5₂₋₃} submembers are significantly more enriched in these two elements than the dolostones in the Ma₅ submember. As shown in Figure 6, the Mn/Ca and Fe/Ca ratios of the Ma₅ submember are smaller than that of the Ma_{5₂₋₃} submember, indicating that the Ma₅ submember in the shallow burial zone beneath the phreatic surface was slightly modified by Fe-rich meteoric water. This result is consistent with the fracture phenomenon observed in the core, indicating that Ma_{5₁₋₂} submember and Ma_{5₃₋₄} submember are in the vertical vadose zone and horizontal phreatic zone.

When using elemental geochemistry for this discussion, it is necessary to first verify whether the sample has been modified by diagenesis, and (Kaufman et al., 1992; Kaufman et al., 1993) gave an upper limit of 2–3 for Mn/Sr ratios for well research samples, and the Mn/Sr ratios for the Daniudi samples are generally in this range (0.34–2.37), except for a few samples from one well (PG27). The diagenetic paleoenvironment of dolomite can be analyzed according to rare earth elements. Dolomite with seawater origin is rich in light rare earth elements and poor in heavy rare earth elements (Banner et al., 1988; Kamber and

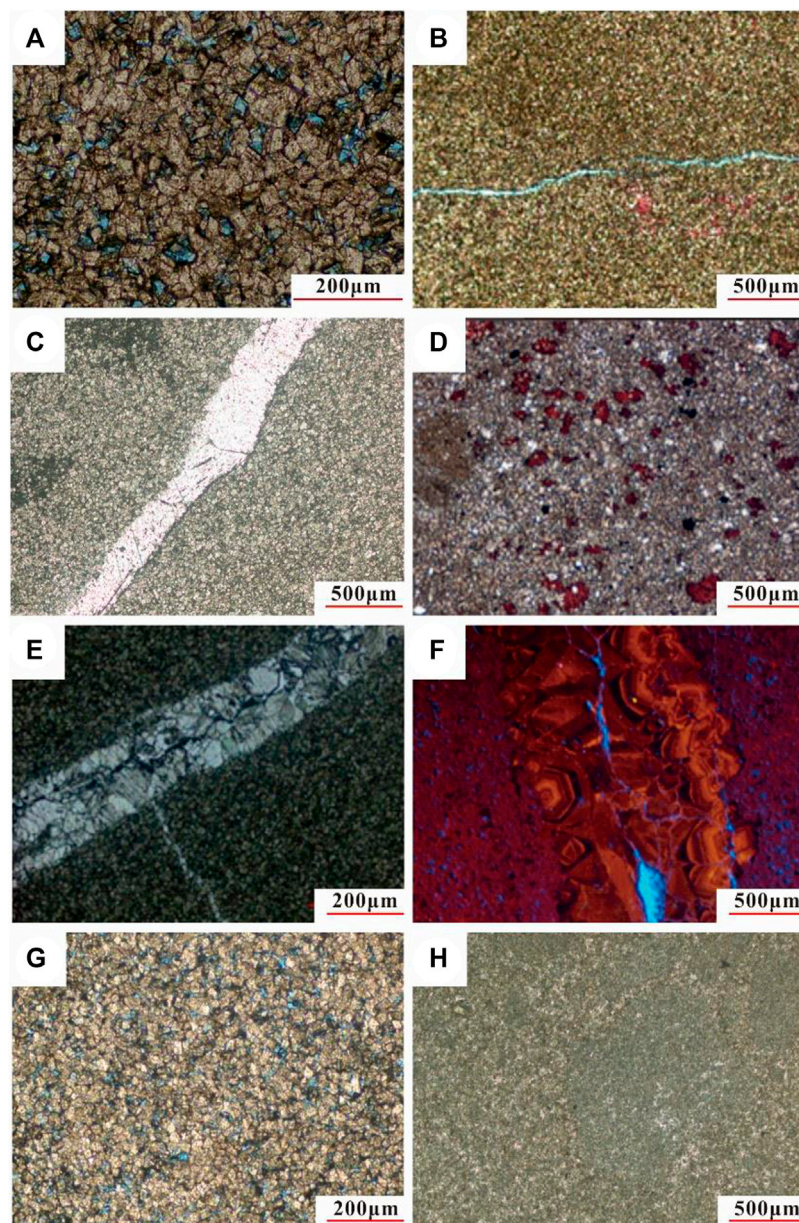


FIGURE 11

Microscopic photos of pores and fractures. (A) Well D30, 3022.42 m, intercrystalline pore in very fine crystalline dolomite; (B) Well D1-530, 3113.46 m, microfracture; (C) Well PG27, 2977.71 m, calcite cement of fracture; (D) Well D48, 3013.0 m, gypsum-shaped pores filled with calcite; (E) Well D48, 3009.32 m, fractures filled with calcite; (F) Well D48, 3018.10 m, cathodoluminescence photo, the minerals with blue color are fluorites filling in the karstfracture; (G) Well D30, 3021.57 m, intercrystalline pore in very fine crystalline dolomite; (H) Well PG27, 2995.6 m, micritic dolomite without any pore space.

Webb, 2001; Nothdurft et al., 2004; Yang et al., 2018). Previous studies believe that the negative Eu anomaly can indicate the low temperature alkaline diagenetic environment (Frimmel, 2008; He et al., 2014), while the negative Ce anomaly can reflect the oxidation degree of the diagenetic environment. According to the REEs pattern of the sample after standardization of North American shale (Figure 7), the diagenetic environment of

micritic dolomite and very fine crystalline dolomite was under the low temperature and alkaline fluid. The diagenetic environment of very fine crystalline dolomite was under weak oxidation. The redox condition can reflect the degree of opening of the diagenetic environment. The REEs patterns of these samples indicate that the dolomitized fluid is closely related to seawater. The micritic dolomite was formed in the restricted

Diagenetic stage	Penecontemporaneous stage	Supergene stage	Early diagenetic stage	Late diagenetic stage
	Near-surface	Shallow buried	Surface	Depth buried
Compaction		—————		
Dolomitization	—————	—————		
Gypsum		—————		
Pressolution		—————		
Meteoric water dissolution			—————	
Meteoric freshwater calcite			—————	
Demineralization			—————	
Clay minerals			—————	
Burial dissolution				—————
Burial filling				—————
Fracturing			—————	—————

FIGURE 12
The paragenesis of carbonate rocks in the Ma5₅ submember.

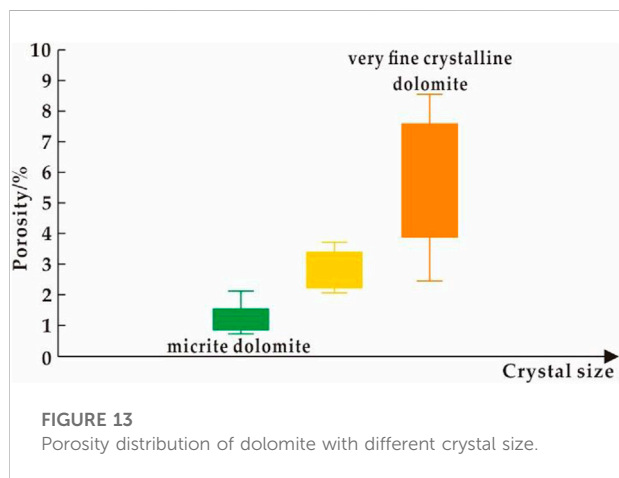


FIGURE 13
Porosity distribution of dolomite with different crystal size.

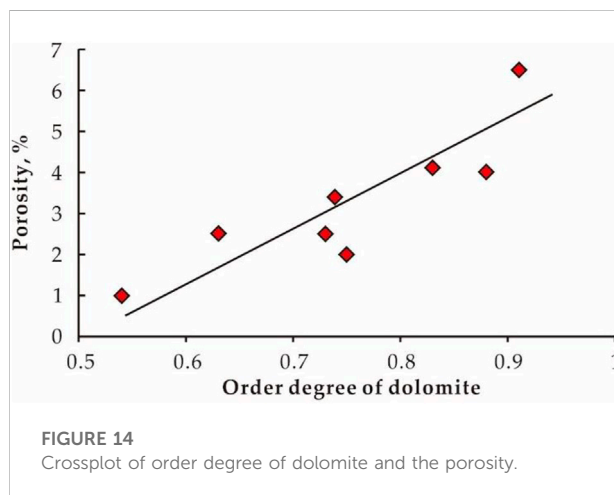


FIGURE 14
Crossplot of order degree of dolomite and the porosity.

environment with high salinity, while the very fine crystalline dolostone was dolomitized in the shallow burial environment.

Sr isotope, C and O isotope can reflect the salinity of dolomitized fluid (Swart et al., 1987; Compton et al., 2001; Yuan et al., 2015; Bi et al., 2018; Jiang et al., 2019; Bai et al., 2022), but these isotopes could be modified during the burial diagenesis or exposure erosion. The calcite precipitated during subaerial exposure with the zonal cathodoluminescence has the lightest C and O isotope values. The $\delta^{18}\text{O}_{\text{V-PDB}}$ values of very fine

crystalline dolomite and micritic dolomite are similar (-8.43 – -6.34%) (Figure 8), partly less than -8% . The C and O isotopes show that the diagenetic environment of micritic dolomite and very fine crystalline dolomite was weakly influenced by meteoric water. On the other hand, the ratio of $^{87}\text{Sr}/^{86}\text{Sr}$ of all samples is slightly higher than that of contemporary seawater (Figure 9). Although the average $^{87}\text{Sr}/^{86}\text{Sr}$ value of very fine crystalline dolomite is slightly lower than that of micritic dolomite and similar to limestone, the Sr isotopes

of the two types of dolomite show that they were weakly influenced by meteoric water during the subaerial exposure.

Based on the analysis of strontium isotope, C and O isotope data and major elements, it is considered that the dolostones in the Ma5₅ submember in the shallow burial zone beneath the phreatic surface were slightly modified by meteoric water.

5.2 Reservoir quality of dolostones in the shallow burial zone beneath the phreatic surface

Through thin section identification, the very fine crystalline dolostones in the Ma5₅ submember have a small number of pores: with the average area percentage of pore under microscope of 1.5%. However, the micritic dolostones almost have no visible pores. As shown in Figure 10, the porosity of carbonate rocks in the Ma5₅ submember mainly ranges from 1% to 3%, and the permeability mainly ranges from 0.01 to $0.05 \times 10^{-3} \mu\text{m}^2$. The void spaces of the carbonate reservoirs are dominated by intercrystalline pores (Figure 11A), with minor microfractures (Figure 11B). In addition, two types of invalid void spaces have been observed, e.g., gypsum mold holes completely filled with calcite, and weathering fractures filled with calcite. These void spaces formed in the early meteoric water dissolution, and destroyed by late cementation.

With the proceeding of dolomitization under shallow burial environment, the new void spaces will be created by replacement in very fine crystalline dolomites. Meanwhile, because the very fine crystalline dolomites are located in shallow burial zone beneath the phreatic surface, calcium-rich fluids from the upper phreatic zone may penetrate into the reservoir after subaerial dissolution along weathering fractures and then result in strengthened cementation, which 100% filled the dissolution fractures in early diagenesis and destroyed the reservoir space (Figure 11C). The effective fractures observed under the microscope are regular fractures, with the average percentage of area of 0.4%. According to the petrography characteristic, fractures without fillings formed in the late diagenesis.

In addition to the two types of effective void spaces, gypsum-shaped holes full filled with calcite (Figure 11D) and karst-fractures filled with calcite and fluorite (Figures 11C, E, F) were also observed, but neither of them had reservoir properties. In the sedimentary period of the Ma5₅ submember, the gypsum precipitated in the west of the study area, which was a restricted environment. During the subaerial exposure, weathering fractures and small branching dissolution fractures developed with the dissolution of meteoric water. As the soluble minerals in meteoric water, gypsum dissolved to form pores and caves. On the other hand, because of Ca-rich fluid formed in the vadose zone and phreatic zone after subaerial dissolution, there were a large number of calcites

precipitated in pores and caves in the shallow burial zone beneath the phreatic surface, leading to the destruction of gypsum-shaped pores and caves. Large-scale cementation in the subaerial exposure and burial cementation resulted in the complete filling in gypsum-shaped dissolved pores and karst-fractures (Figures 11C–E). Therefore, we suggest that the meteoric water during the subaerial exposure has little effect on the quality of carbonate reservoir in the shallow burial zone beneath the phreatic surface.

5.3 Main controlling factors of reservoirs quality in the Ma5₅ submember

Previous studies have divided multiple types of reservoirs in the Ma5₅ submember based on karstification (Liu et al., 2014; Wu et al., 2015). As discussed above, the influence of meteoric water during the subaerial exposure on the carbonate reservoirs in the Ma5₅ submember is obviously weaker than that in the upper stratas in vadose zone and phreatic zone. There is a large scale of dolostones developed in the Ma5₅ submember. The main controlling factors of reservoir quality in the Ma5₅ submember can be analyzed combined with the influence of meteoric water on the dolostones in the shallow burial zone beneath the phreatic surface.

Based on the above discussion, this study established a paragenesis of carbonate reservoirs in the Ma5₅ submember (Figure 12). The diagenetic alterations include pencontemporaneous/shallow burial dolomitization—meteoric water dissolution—shallow burial cementation—middle-deep burial cementation—late tectonic fracture. The main controlling factor for reservoir development was dolomitization, resulting in the formation of high-quality reservoirs. According to the above analysis of isotope and element, the dolomitization mechanism includes evaporative pump dolomitization with rapid crystallization and seepage-reflux dolomitization. During the regressive period of the Ma5₅ submember, the deposition environment changed into a restricted evaporative tidal flat, and the Mg/Ca ratio of the diagenetic fluid increased rapidly with the precipitation of gypsum. The abundant Mg²⁺ rich fluid sources improved the pencontemporaneous dolomitization of mud lime and then micritic dolomite formed. In contrast, the dolomitization in the subtidal zone occurred in the shallow burial stage, with the reflux of brine from the supratidal zone.

The statistics of porosity in different crystal size dolomite indicated that the upper porosity of the very fine crystalline dolomite is the highest (Figure 13). The crystal size of dolomite is closely related to the degree of order of dolomite, and both of them are also related to physical properties (Ma et al., 2007; Shen et al., 2016), as shown in Figure 14, there was a positive correlation between the order degree of the dolomite and porosity of the reservoir rocks. Due to the difference of

crystallization environment and crystallization rate, the crystal sizes of dolomites can influence the physical properties (Figures 11G, H). As mentioned above, micritic dolostone has few pores, while very fine crystalline dolomite has well-developed pore space. After the deposition, the carbonate rocks in Ma5₁₋₄ submember in the study area were exposure and karstification during the Caledonian Orogeny. However, since the Ma5₅ submember was distributed in the shallow burial zone beneath the phreatic surface, the effect of meteoric water on the reservoir physical property of the Ma5₅ submember was relatively weak. Although the meteoric water dissolution could be identified in the Ma5₅ submember, a large-scale cementation occurred in the Ma5₅ submember. The original pore—fracture system become the fluid flow channel. Due to the strong dissolution in the vadose zone and the phreatic zone, the overlying diagenetic fluid enriched in Ca²⁺ entered into dolostones in the Ma5₅ submember under gravity along early fractures. The retention of Ca-rich fluid in shallow burial zones beneath the phreatic surface result in a large number of calcite precipitation. The few reservoir spaces formed by the meteoric water dissolution were filled again. Due to the Ca-rich fluid cannot flow through the intercrystalline pores with small volume and throat radius, resulting in the weak cementation occurred in the very fine crystalline dolostones, the tiny fracture was preserved (Figure 11B). In addition, as the main fluid flow channel, the weathering fractures were filled by calcite in the shallow burial cementation, as well as the fluorite in the late diagenetic cementation (Figures 11C, E, F). Furthermore, tectonic fracture formed in the late diagenetic period can improve the permeability of the reservoirs. As a result, the development of high-quality dolostone reservoirs was mainly controlled by dolomitization, and the very fine crystalline dolostones are the high-quality reservoirs in the Ma5₅ submember in the shallow burial zone beneath the phreatic surface.

6 Conclusion

- (1) There are two types of dolostones in the Ma5₅ submember of Daniudi Gas Field, i.e., micrite dolostone and very fine crystalline dolostone. The very fine crystalline dolostone are the reservoirs with high-quality developed in the Ma5₅ submember.
- (2) These dolostone reservoirs distributed in the shallow burial zone beneath the phreatic surface were slightly modified by meteoric fresh water, with evidences from Mn/Ca, Fe/Ca, Sr and O isotope.
- (3) The main controlling factors of the very fine crystalline dolostone reservoirs was dolomitization. The dissolved pores and fractures created by meteoric water dissolution were filled again in the late cementation in the shallow burial zone.

Data availability statement

The original contributions presented in the study are included in the article/supplementary material, further inquiries can be directed to the corresponding authors.

Author contributions

HL: Data curation, writing-original draft preparation and writing-review and editing; MG: Conceptualization, formal analysis, writing-review and editing, visualization and project administration; MF: Conceptualization, methodology, formal analysis, writing-review and editing, visualization and project administration; HD: Methodology, validation and supervision; JG: Writing-review and editing; WX: Software and validation; MT: Resources and funding acquisition; DW: Investigation; YL: Validation; HG: Investigation.

Funding

This work is funded by the Exploration and Development Research Institute (SINOPEC North China Oil and Gas Company, China) (Grant No. 80303-AHD050).

Acknowledgments

We thank Exploration and Development Research Institute of North China Oil and Gas Company, SINOPEC.

Conflict of interest

MT was employed by Exploration and Development Research Institute of North China Oil and Gas Company.

The remaining authors declare that the research was conducted in the absence of any commercial or financial relationships that could be construed as a potential conflict of interest.

The authors declare that this study received funding from North China Oil and Gas Company, SINOPEC. The funder was not involved in the study design, collection, analysis, interpretation of data, the writing of this article, or the decision to submit it for publication.

Publisher's note

All claims expressed in this article are solely those of the authors and do not necessarily represent those of their affiliated organizations, or those of the publisher, the editors and the reviewers. Any product that may be evaluated in this article, or claim that may be made by its manufacturer, is not guaranteed or endorsed by the publisher.

References

- Bai, Y., Liu, W., and Xu, W. L. (2022). Dolomite Genesis and dolomitization mechanisms of the ordovician lower yingshan formation, gucheng area, tarim basin, China. *J. Pet. Sci. Eng.* 215, 110570. doi:10.1016/j.petrol.2022.110570
- Banner, J. L., Hanson, G. N., and Meyers, W. J. (1988). Rare Earth element and Nd isotopic variations in regionally extensive dolomites from the burlington-keokuk formation (mississippian): Implications for REE mobility during carbonate diagenesis. *J. Sediment. Petrol.* 58 (3), 415–432. doi:10.1306/212F8DAA-2B24-11D7-8648000102C1865D
- Bi, D. J., Zhai, S. K., Zhang, D. J., Liu, X. F., Liu, X. Y., Jiang, L. J., et al. (2018). Constraints of fluid inclusions and C, O isotopic compositions on the origin of the dolomites in the Xisha Islands, South China Sea. *Chem. Geol.* 493, 504–517. doi:10.1016/j.chemgeo.2018.07.005
- Chen, J. S., Li, Z., Wang, Z. Y., Tan, X. C., Li, L., and Ma, Q. (2007). Paleokarstification and reservoir distribution of ordovician carbonates in tarim basin. *Acta Sedimentol. Sin.* 6, 858–868. doi:10.3969/j.issn.1000-0550.2007.06.007
- Compton, J. S., Harris, C., and Thompson, S. (2001). Pleistocene dolomite from the Namibian shelf: High $^{87}\text{Sr}/^{86}\text{Sr}$ and ^{18}O values indicate an evaporative, mixed-water origin. *J. Sediment. Res.* 71 (5), 800–808. doi:10.1306/2DC40969-0E47-11D7-8643000102C1865D
- Ding, Z. W., Wang, R. J., Chen, F. F., Yang, J. P., Zhu, Z. Q., Yang, Z. M., et al. (2020). Origin, hydrocarbon accumulation and oil-gas enrichment of fault-karst carbonate reservoirs: A case study of ordovician carbonate reservoirs in south tahe area of halahatang oilfield. *Tarim. Basin. Pet. Explor. Dev. Online.* 47 (2), 286–296. doi:10.11698/PED.2020.02.07
- Esteban, M. (1991). Paleokarst facies analysis: General trends and cretaceous occurrences. *AAPG Bull.* 75 (11), 1805. doi:10.1007/s12517-016-2634-0
- Feng, Z. Z. (1992). Single factor analysis and multifactor comprehensive mapping method—reconstruction of quantitative lithofacies paleogeography. *J. Palaeogeogr.* 1, 3–19. doi:10.3969/j.issn.1671-1505.2004.01.002
- Frimmel, H. E. (2008). Trace element distribution in Neoproterozoic carbonates as palaeo-environmental indicator. *Chem. Geol.* 258 (3–4), 338–353. doi:10.1016/j.chemgeo.2008.10.033
- Fu, J. H., Wu, X. N., Sun, L. Y., Yu, Z., Huang, Z. L., and Ding, Z. C. (2017). New understandings of the lithofacies paleogeography of the middle assemblage of Majiagou Fm in the Ordos Basin and its exploration significance. *Nat. Gas. Ind.* 37, 278–286. doi:10.1016/j.ngib.2017.08.011
- Fu, S. Y., Zhang, C. G., Chen, H. D., Chen, A. Q., Zhao, J. X., Su, Z. T., et al. (2019). Characteristics, formation and evolution of pre-salt dolomite reservoirs in the fifth member of the Ordovician Majiagou Formation, mid-east Ordos Basin, NW China. *Pet. Explor. Dev.* 46 (6), 1153–1164. doi:10.1016/S1876-3804(19)60270-3
- Gromet, L. P., Haskin, L. A., Korotev, R. L., and Dymek, R. F. (1984). The “North American shale composite”: Its compilation, major and trace element characteristics. *Geochim. Cosmochim. Acta.* 48 (12), 2469–2482. doi:10.1016/0016-7037(84)90298-9
- He, J., Fang, S. X., Hou, F. H., Yan, R. H., Zhao, Z. J., Yao, J., et al. (2013). Vertical zonation of weathered crust ancient karst and reservoir evaluation and prediction—a case study of M5₅–M5₁ sub-members of Majiagou Formation in gas fields, central Ordos Basin, NW China. *Pet. Explor. Dev. Online.* 40 (5), 572–581. doi:10.1016/S1876-3804(13)60075-0
- He, X. Y., Shou, J. F., Shen, A. J., Wu, X. N., Wang, Y. S., Hu, Y. Y., et al. (2014). Geochemical characteristics and origin of dolomite: A case study from the middle assemblage of ordovician Majiagou Formation member 5 of the west of jingbian gas field, Ordos Basin, North China. *Pet. Explor. Dev.* 41 (3), 417–427. doi:10.1016/S1876-3804(14)60048-3
- Henry, S. C., Imerito-Tetzlaff, A. A., and Jilin, Z. (1999). Stable-isotope and elemental trends in Pleistocene sabkha dolomites, descending meteoric water vs. sulfate reduction. *J. Sediment. Res.* 69 (1), 256–266. doi:10.2110/j.sr.69.256
- Hou, F. H., Fang, S. X., Dong, Z. X., Zhao, J. S., Lu, S. X., Wu, Y., et al. (2003). The developmental characters of sedimentary environments and lithofacies of middle ordovician Majiagou Formation in Ordos Basin. *Acta Sedimentol. Sin.* 01, 106–112. doi:10.14027/j.cnki.cjxb.2003.01.016
- Huang, S. J. (1990). Cathodoluminescence and diagenetic alteration of marine carbonate minerals. *Sediment. Geol. Tethyan Geol.* 4, 9–15.
- Jiang, C. L., and Jin, Z. K. (2009). Study on karst facies of Cambrian-Ordovician strata in Tazhong area. *J. Oil Gas. Technol.* 31 (5), 161–165. CNKI:SUN:JHSX.0.2009-05-042.
- Jiang, W. J., Hou, M. C., and Chao, W. (2019). Strontium isotopic compositions of Cambrian (Upper Miaolingian–Furongian Series) dolomites from south-eastern Sichuan Basin, China: Significance of sources of dolomitizing fluids and timing of dolomitization. *Mar. Pet. Geol.* 109, 408–418. doi:10.1016/j.marpetgeo.2019.06.042
- Jiu, B., Huang, W. H., Mu, N. N., and Li, Y. (2021). Types and controlling factors of ordovician paleokarst carbonate reservoirs in the southeastern Ordos Basin, China. *J. Pet. Sci. Eng.* 198, 108162. doi:10.1016/j.petrol.2020.108162
- Kamber, B. S., and Webb, G. E. (2001). The geochemistry of late archaean microbial carbonate: Implications for ocean chemistry and continental erosion history. *Geochim. Cosmochim. Acta.* 65, 2509–2525. doi:10.1016/S0016-7037(01)00613-5
- Kaufman, A. J., Jacobsen, S. B., and Knoll, A. H. (1993). The vendian record of Sr and C isotopic variations in seawater: Implications for tectonics and paleoclimate. *Earth Planet. Sci. Lett.* 120 (3–4), 409–430. doi:10.1016/0012-821X(93)90254-7
- Kaufman, A. J., Knoll, A. H., and Awramik, S. M. (1992). Biostratigraphic and chemostratigraphic correlation of Neoproterozoic sedimentary successions: Upper Tindir Group, northwestern Canada, as a test case. *Geology* 20 (02), 181–185. doi:10.1130/0091-7613(1992)020<0181:baccon>2.3.co;2
- Lei, B. J., Lu, T., Wang, D. X., Wang, Y., Li, S. L., and Gu, S. F. (2010). Research on the sedimentary microfacies and diageneses of ma5₁₋₄ submember in jingbian gas field. *Acta Sedimentol. Sin.* 28 (06), 1153–1164. doi:10.14027/j.cnki.cjxb.2010.06.020
- Li, J., Zhang, W. Z., Luo, X., and Hu, G. Y. (2008). Paleokarst reservoirs and gas accumulation in the Jingbian field, Ordos Basin. *Mar. Pet. Geol.* 25 (4–5), 401–415. doi:10.1016/j.marpetgeo.2008.01.005
- Li, W., Tu, J. Q., Zhang, J., and Zhang, B. (2017). Accumulation and potential analysis of self-sourced natural gas in the ordovician Majiagou Formation of Ordos Basin, NW China. *Pet. Explor. Dev.* 44 (4), 552–562. doi:10.1016/S1876-3804(17)30064-2
- Lin, P., Peng, J., Zhang, L. J., Lan, X. M., Wang, J. J., Xia, Q. S., et al. (2022). Characteristics of multiple dolomitizing fluids and the genetic mechanism of dolomite formation in the Permian Qixia Formation, NW Sichuan Basin. *J. Pet. Sci. Eng.* 208, 0920–4105. doi:10.1016/j.petrol.2021.109749
- Liu, J. D., Hang, Y. L., Liu, X. S., Yang, Z. W., Hou, X. D., Zhu, R. W., et al. (2017). Genesis of dolomite from ma5₅–ma5₁₀ sub-members of the ordovician Majiagou Formation in the jingxi area in the Ordos Basin. *Acta Geol. Sin. Engl. Ed.* 91 (4), 1363–1379. doi:10.1111/1755-6724.13367
- Liu, M., Ding, X. Q., Wang, Y. L., Bai, X. L., Chen, Q. Q., and Le, J. P. (2014). Characteristics and distribution of ordovician weathering crust reservoirs in Daniudi gas field, Ordos Basin. *Mar. Orig. Pet. Geol.* 19 (1), 35–42. doi:10.3969/j.issn.1672-9854.2014.01.005
- Liu, X. Y., Wei, L. B., Liu, B. X., Zhang, L., Guo, W., Zhang, J. W., et al. (2021). Characteristics of natural gas accumulation in the Cambrian weathering crust in the southwestern Ordos Basin. *Nat. Gas. Ind.* 41 (4), 13–21. doi:10.3787/j.issn.1000-0976.2021.04.002
- Luo, Z. F., Su, Z. T., Liao, H. H., Huang, W. M., Ma, H., and She, W. (2022). Characteristics and geological significance of stromatolite dolomite of Ma5₅ submember of ordovician Majiagou Formation in mizhi area, central-eastern Ordos Basin. *Lithol. Reserv.* 34 (2), 86–94. doi:10.12108/xyyqc.20220208
- Ma, Y. S., Guo, T. L., Zhao, X. F., and Cai, X. Y. (2007). Formation mechanism of deep quality dolomite reservoir in Puguang Gas Field. *Sci. Sin.* 37 (2), 43–52. doi:10.3321/j.issn:1006-9267.2007.z2.005
- Muchez, N., Sintubin, L., Sintubin, M., and Lagrou, D. (1998). Conditions of meteoric calcite formation along a Variscan fault and their possible relation to climatic evolution during the Jurassic–Cretaceous. *Sedimentology* 45 (5), 845–854. doi:10.1046/j.1365-3091.1998.00182.x
- Nothdurft, L. D., Webb, G. E., and Kamber, B. S. (2004). Rare Earth element geochemistry of late devonian reefal carbonates, cannning basin, western Australia: Confirmation of a seawater REE proxy in ancient limestones. *Geochim. Cosmochim. Acta.* 68 (2), 263–283. doi:10.1016/S0016-7037(03)00422-8
- Popp, B. N., Anderson, T. F., and Sandberg, P. A. (1986). Brachiopods as indicators of original isotopic compositions in some Paleozoic limestones. *Geol. Soc. Am. Bull.* 97 (10), 1262–1269. doi:10.1130/0016-7606(1986)97<1262:BAIOOI>2.0.CO;2
- Qu, Q. G., Zhang, J. X., Lu, Y. M., and Zhu, F. Y. (2015). Vertical zoning of karst formations in reservoirs with thick limestones: A case study of district 4 in tahe oilfield. *Pet. Geol. Exp.* 37 (01), 17–21. doi:10.11781/sysydz201501017
- Retana, A. E. B., Bruna, V. L., Rustichelli, A. C., Bezerra, F. H. R., Xavier, M. M., Audra, P., et al. (2021). Structural and sedimentary discontinuities control the generation of karst dissolution cavities in a carbonate sequence, Potiguar Basin, Brazil. *Mar. Pet. Geol.* 123, 104753. doi:10.1016/j.marpetgeo.2020.104753
- Shen, A. J., Zheng, J. F., Chen, Y. Q., Ni, X. F., and Huang, L. L. (2016). Characteristics, origin and distribution of dolomite reservoirs in lower-middle

cambrian, tarim basin, NW China. *Pet. Explor. Dev.* 43 (03), 375–385. doi:10.1016/s1876-3804(16)30044-1

Sun, Y. J. (2020). *Study on characteristics and main controlling factors of karst reservoir in Ma5₁- Ma5₄ submember in Northeast part, Ordos Basin*. Xi'an: Northwest University.

Swart, P. K., Ruiz, J., and Holmes, C. W. (1987). Use of strontium isotopes to constrain the timing and mode of dolomitization of upper Cenozoic sediments in a core from San Salvador, Bahamas. *Geology* 15 (3), 262–265. doi:10.1130/0091-7613(1987)15<262:uositc>2.0.co;2

Veizer, J., Ala, D., Azmy, K., Bruckschen, P., Buhl, D., Bruhn, F., et al. (1999). ⁸⁷Sr/⁸⁶Sr, δ¹³C and δ¹⁸O evolution of Phanerozoic seawater. *Chem. Geol.* 161 (1-3), 1586–1588. doi:10.1180/minmag.1998.62a.3.165

Wang, X. L., Wang, C. L., Chen, Z. L., and Tian, J. J. (2005). Study of Ordovician weathering crust karst reservoirs in Ordos Basin. *Spec. Oil Gas. Reserv.* 3, 32–35+108. doi:10.3969/j.issn.1006-6535.2005.03.010

Wei, X. S., Chen, H. D., Zhang, D. F., Dai, R., Guo, Y. R., Chen, J. P., et al. (2017). Gas exploration potential of tight carbonate reservoirs: A case study of ordovician Majiagou Formation in the eastern yi-Shan slope, Ordos Basin, NW China. *Pet. Explor. Dev.* 44 (3), 347–357. doi:10.1016/s1876-3804(17)30041-1

Wei, X. S., Ren, J. F., Zhao, J. X., Zhang, D. F., Luo, S. S., Wei, L. B., et al. (2018). Paleogeomorphology evolution of the Ordovician weathering crust and its implication for reservoir development, eastern Ordos Basin. *Pet. Res.* 3 (1), 77–89. doi:10.1016/j.ptlrs.2018.03.004

Wennberg, O. P., Casini, G., Jonoud, S., and Peacock, D. C. P. (2016). The characteristics of open fractures in carbonate reservoirs and their impact on fluid flow: A discussion. *Pet. Geosci.* 22 (1), 91–104. doi:10.1144/petgeo2015-003

Wu, Y. F., Lei, T., Liu, X. G., and Gui, P. J. (2015). Reservoir characteristics and development controlling factors of Ordovician weathering crust in Daniudi gas field. *Pet. Geol. Eng.* 29 (3), 1–5+145. doi:10.3969/j.issn.1673-8217.2015.03.001

Xiao, D., Tan, X. C., Fan, L. Y., Zhang, D. F., Nie, W. C., Niu, T., et al. (2019). Reconstructing large-scale karst paleogeomorphology at the top of the Ordovician in the Ordos Basin, China: Control on natural gas accumulation and paleogeographic implications. *Energy Sci. Eng.* 7 (6), 3234–3254. doi:10.1002/ese3.494

Xie, K., Tan, X. C., Feng, M., Wang, B. B., Zhong, S. K., Yang, M., et al. (2020). Eogenetic karst and its control on reservoirs in the ordovician Majiagou Formation, eastern sulige gas field, Ordos Basin, NW China. *Pet. Explor. Dev.* 47 (6), 1246–1261. doi:10.1016/S1876-3804(20)60133-7

Xie, R. C., Zhou, W., Zhang, C., Lei, T., Yin, S., and Luo, Z. W. (2020). Characteristics, influencing factors, and prediction of fractures in weathered crust karst reservoirs: A case study of the ordovician Majiagou Formation in the Daniudi gas field, Ordos Basin, China. *Geol. J.* 55 (12), 7790–7806. doi:10.1002/gj.3907

Xu, X., Feng, Q. H., Wei, Q. S., Yang, S. G., Zhang, J. C., Pang, Q., et al. (2021). Sedimentary characteristics and reservoir origin of the mound and shoal microfacies of the Ma5₁₊₂ submember of the Majiagou Formation in the Jingbian area. *J. Pet. Sci. Eng.* 196, 108041. doi:10.1016/j.petrol.2020.108041

Yang, H., Fu, J. H., Wei, X. S., and Ren, J. F. (2011). Natural gas exploration domains in Ordovician marine carbonates Ordos Basin. *Acta Pet. Sin.* 32(5), 733–740. doi:10.7623/syxb201105001

Yang, M. Y., Tan, X. C., Yang, M. Y., Xu, Y. Q., Yan, W., Su, W. J., et al. (2021). Basin-scale distribution and dominant controlling factors of microbialites of the Ma5₅ sub-member of ordovician Majiagou Formation in Ordos Basin. *J. Palaeogeogr.* 23 (6), 1125–1139. doi:10.7605/gdxb.2021.06.072

Yang, W., Wei, G. Q., Xie, W. R., Liu, M. C., Su, N., Jin, H., et al. (2021). Role of paleouplift in the scale formation of intra-platform carbonate mound-bank body reservoirs in the Sichuan Basin. *Nat. Gas. Ind.* 41 (4), 443–454. doi:10.1016/j.ngib.2021.08.003

Yang, X. Y., Mei, Q. Y., Wang, X. Z., Dong, Z. X., Li, Y., and Huo, F. (2018). Indication of rare Earth element characteristics to dolomite petrogenesis—a case study of the fifth member of ordovician Majiagou Formation in the Ordos Basin, central China. *Mar. Pet. Geol.* 92, 1028–1040. doi:10.1016/j.marpetgeo.2017.12.004

Yu, Z., Zhou, J. G., Ding, Z. C., Wei, L. B., Wei, Y., Wu, X. N., et al. (2020). Reservoir characteristics and Genesis of the ordovician Ma5₄₋₁ in the central and eastern parts of the Ordos Basin, China. *Nat. Gas. Geosci.* 5 (5), 285–297. doi:10.1016/j.jnggs.2020.09.001

Yuan, J. Y., Huang, C. G., Zhao, F., and Pan, X. (2015). Carbon and oxygen isotopic compositions, and palaeoenvironmental significance of saline lacustrine dolomite from the Qaidam Basin, Western China. *J. Pet. Sci. Eng.* 135, 596–607. doi:10.1016/j.petrol.2015.10.024

Zhang, J., Brian, J., and Zhang, J. Y. (2014). Crystal structure of replacement dolomite with different buried depths and its significance to study of dolomite reservoir. *China Pet. explor.* 19 (3), 21–28. doi:10.3969/j.issn.1672-7703.2014.03.003

Zhang, S., Jin, Q., Sun, J. F., Wei, H. H., Cheng, F. Q., and Zhang, X. D. (2021). Formation of hoodoo-upland on Ordovician karst slope and its significance in petroleum geology in Tahe area, Tarim Basin, NW China. *Pet. Explor. Dev.* 48 (2), 354–366. doi:10.1016/S1876-3804(21)60028-9

Zhang, Y. P., Lv, X. X., Yu, H. F., Jing, B., Zhang, C. L., and Cai, J. (2016). Controlling mechanism of two strike-slip fault groups on the development of the Ordovician karst reservoirs in the Tazhong Uplift, Tarim Basin. *Oil Gas. Geol.* 37 (5), 663–673. doi:10.11743/ogg20160506

Zhao, H. T., Wang, Z. Q., and Liu, J. (2019). Main diagenesis of middle-lower ordovician of yubei area in tarim basin. *Earth Sci.* 8 (6), 352–358. doi:10.11648/j.earth.20190806.16

Zhong, Q. Q., Huang, S. J., Zou, M. L., Dong, H. P., Huang, K. K., and Zhang, X. H. (2009). Controlling factors of order degree of dolomite in carbonate rocks: A case study from lower paleozoic in tahe oilfield and triassic in northeastern sichuan basin. *Lithol. Reserv.* 21 (3), 50–55. doi:10.3969/j.issn.1673-8926.2009.03.010

Zhu, D. C., Zou, H. Y., Yang, M. L., Li, T., Li, T., Li, H. P., et al. (2021). The middle permian maokou reservoir (southern sichuan basin, China): Controls on karst development and distribution. *J. Pet. Sci. Eng.* 204, 108686. doi:10.1016/j.petrol.2021.108686

Zhu, L. W., Wang, Z. L., Zhang, B., Wei, L., Feng, Q. H., Lei, X., et al. (2018). Characteristics of paleogeomorphology and paleokarstification and the impact on natural gas accumulation: A case study of upper assemblage of Majiagou Formation in central sulige gas field, Ordos Basin, China. *China. Carbonates Evaporites* 34 (4), 1353–1366. doi:10.1007/s13146-018-0434-1